Received: 7 July 2023 | Accepted: 27 December 2023
DOI: 10.1002/ame2.12383

ORIGINAL ARTICLE

C1ql3 knockout affects microglia activation, neuronal integrity, and spontaneous behavior in Wistar rats

Li Zhang[1] | **Wei Dong**[2] | **Jingwen Li**[2] | **Shan Gao**[2] | **Hanxuan Sheng**[2] | **Qi Kong**[2] | **Feifei Guan**[1] | **Lianfeng Zhang**[2,3]

[1]Beijing Engineering Research Center for Experimental Animal Models of Human Diseases, Institute of Laboratory Animal Science, Peking Union Medicine College, Chinese Academy of Medical Sciences, Beijing, China

[2]Key Laboratory of Human Disease Comparative Medicine, National Health Commission of China (NHC), Institute of Laboratory Animal Science, Peking Union Medicine College, Chinese Academy of Medical Sciences, Beijing, China

[3]Neuroscience Center, Chinese Academy of Medical Sciences, Beijing, China

Correspondence
Lianfeng Zhang and Feifei Guan, Institute of Laboratory Animal Science, Peking Union Medicine College, Chinese Academy of Medical Sciences, Building 5, Panjiayuan Nanli, Chaoyang District, Beijing 100021, China.
Email: zhanglf@cnilas.org and guanff@cnilas.org

Funding information
National Natural Science Foundation of China, Grant/Award Number: 31970508; National Key Research and Development Program of China, Grant/Award Number: 2022YFF0710702

Abstract

Background: C1QL3 is widely expressed in the brain and is specifically produced by a subset of excitatory neurons. However, its function is still not clear. We established *C1ql3*-deficient rats to investigate the role of C1QL3 in the brain.

Methods: *C1ql3* knockout (KO) rats were generated using CRISPR/Cas9. *C1ql3* KO was determined by polymerase chain reaction (PCR), DNA sequencing, and western blotting. Microglia morphology and cytokine expression with or without lipopolysaccharide (LPS) stimulus were analyzed using immunohistochemistry and real-time PCR. The brain structure changes in KO rats were examined using magnetic resonance imaging. Neuronal architecture alteration was analyzed by performing Golgi staining. Behavior was evaluated using the open field test, Morris water maze test, and Y maze test.

Results: *C1ql3* KO significantly increased the number of ramified microglia and decreased the number of hypertrophic microglia, whereas *C1ql3* KO did not influence the expression of pro-inflammatory factors and anti-inflammatory factors except IL-10. *C1ql3* KO brains had more amoeboid microglia types and higher Arg-1 expression compared with the WT rats after LPS stimulation. The brain weights and HPC sizes of *C1ql3* KO rats did not differ from WT rats. *C1ql3* KO damaged neuronal integrity including neuron dendritic arbors and spine density. *C1ql3* KO rats demonstrated an increase in spontaneous activity and an impairment in short working memory.

Conclusions: *C1ql3* KO not only interrupts the neuronal integrity but also affects the microglial activation, resulting in hyperactive behavior and impaired short memory in rats, which highlights the role of C1QL3 in the regulation of structure and function of both neuronal and microglial cells.

KEYWORDS
C1QL3, knockout, microglia, neuron, rat

1 | INTRODUCTION

C1q-like subfamily (C1QL) consists of C1QL1–C1QL4, and they are highly and predominantly expressed in the central nervous system (CNS).[1] The C1QLs are secreted proteins, form homomeric or heteromeric complexes, and have been found to be synaptic organizers involved in vital neuronal activities.[2]

C1QL3 is a highly evolutionary conserved gene between humans and rodents and is primarily expressed in adipose tissue and brain tissue.[3] C1QL3 as an adipokine can ameliorate vascular calcification; improve glucose metabolism; and is associated with atherosclerosis,[4] childhood obesity,[5] and type 2 diabetes.[6] In the brain, C1QL3 and C1QL2, released from the mossy fiber-CA3 synapses in the hippocampus (HPC), are likely to modulate kainate-type glutamate receptor–mediated synaptic network activity.[7] In addition, C1QL3 is required for the formation and/or maintenance of the synapses of various brain regions including the basolateral amygdala, the prefrontal cortex, the suprachiasmatic nucleus, and the olfactory bulb and plays a role in fear memory behavior,[8] multiple circadian behaviors,[9] and social transmission of food preference memory.[10]

C1QL3 had been validated as a high-affinity ligand for an adhesion G protein–coupled receptor, BAI3,[11,12] and it was also a possible ligand for kainate receptors including GluK2 and GluK4.[7] Kainate receptors are expressed on neuronal membranes and depolarize on activation by glutamate or other agonists.[13] Not like the kainate receptor, BAI3 is primarily expressed in the brain but is also expressed by other tissues[14,15] and cancer cells, such as lung cancer cells, breast cancer cells, and glioblastoma.[16] A recent study suggested the possible role of C1QL3 in mediating the complex forming between BAI3 and two neuronal pentraxins that may influence excitatory synapses.[17]

Microglia mediate classical innate and adaptive immune responses in the CNS,[18] and it was more appreciated that microglia played key roles in the process of synaptogenesis, synaptic pruning, neurogenesis, and neuronal activity.[18–21] Besides the neuron, C1QL3 was reasonably supposed to target any cells expressing BAI3; however, it was unknown whether the microglia expressed BAI3, which was regulated by C1QL3 in the brain. Here, we showed that primary rat microglia expressed BAI3. *C1ql3* knockout (KO) affected microglia activation from ramified microglia to hypertrophic and amoeboid microglia and increased the expression of anti-inflammatory factor IL-10 in rat brains. And *C1ql3* KO increased the number of amoeboid microglia and the level of anti-inflammatory factor Arg1 after lipopolysaccharide (LPS) stimulus. The neuronal complexity and dendritic spine number were also reduced, which resulted in hyperactive behavior and the damage of short working memory in *C1ql3* KO rats.

2 | MATERIALS AND METHODS

2.1 | Data extraction

The C1QL3 expression in different tissues for humans, rats, and mice was obtained from Expression Atlas (https://asia.ensembl.org).

2.2 | Animals

The *C1ql3* KO rats were established using CRISPR/cas9 following the methods we described previously.[22] The exon 1 of *C1ql3* was targeted with two sgRNAs of (TCATCCTCATCCCGGTGCTGG) and (AAGGTGCTGACAAGAGGGAGG), which, respectively, targeted on the 5′ end and the 3′ end of exon 1. The Cas9 protein (30 ng/μL) and the two sgRNAs (10 ng/μL each) were mixed up, and the sediment was removed by centrifugation. The fertilized eggs from Wistar rats were obtained using the superovulation procedure. The mixture was microinjected into the cytoplasm and male pronucleus of the fertilized eggs and then transferred to pseudo-pregnant Sprague–Dawley (SD) rats. The Wistar litters delivered by the pseudo-pregnant SD rats were genotyped by polymerase chain reaction (PCR) with two upstream primers of (5′-TCCAAAAGCAGACAAGAGGATC-3′ and 5′-CTACTTCTTCACCTACCACGTCCTG-3′) and one downstream primer (5′-GGCTTCTGAAACCTTATACATTCTCG-3′). The gene deletions were confirmed by DNA sequencing analysis, and two founder rats (9 and 13) were selected to be crossed with wild-type (WT) Wistar rats to breed F1 heterozygotes. Finally, founder rat 13 (heterozygous KO) could be passaged and homozygote rats were obtained and used for follow-up studies. The homozygous KO rats were formally named Wistar. C1ql3 (tm)-GC/ILAS in our rat resource website (https://namr.org.cn/Ldesc/1_1074).

2.3 | LPS administration

WT male rats (250–300 g) and *C1ql3* KO male rats (250–300 g) were given an intraperitoneal injection of saline or 5 mg/kg of LPS (Sigma). After 1 week, the rat brains were isolated, and the cortical and HPC brain regions were sectioned for immunohistology.

2.4 | Quantitative real-time-polymerase chain reaction

The human brain samples were obtained from the Human Brain Bank of the Chinese Academy of Medical Sciences & Peking Union Medical College (approval no. 009-2014) as previously described.[23] The fresh rat tissues of the brain, heart, liver, spleen, lung, kidney, thymus, and marrow were obtained from male WT Wister rats. The primary culture microglia and neurons were prepared with the procedure described previously.[24,25] Total RNA in different tissues and cells was isolated by TRIzol reagent (15-596-018, Invitrogen) and was used to prepare cDNA with a reverse transcription kit (RR047A, TaKaRa). Quantitative real-time PCR (qRT-PCR) was performed using SYBGreen RT-PCR kits (RR820A, TaKaRa). The mRNA levels of *C1ql3*, *Bai3*, TNF-α, iNOS, IL-1β, IL-6, Mrc1, IL-10, and Arg1 in different tissues were estimated and normalized to glyceraldehyde 3-phosphate dehydrogenase (GAPDH). The qRT-PCR primers are summarized in Table 1.

TABLE 1 qRT-PCR primers.

Primer name	Sequence
rC1ql3-F	GGCAAGTTCACCTGTTCCAT
rC1ql3-R	TGTTGTTGTTTCCTCCGTGA
hC1ql3-F	GGCATCTACTTCTTCACCTACCA
hC1ql3-R	GAACCACACTGTTACTGGCATAG
rBai3-F	CCAAAAGACCACCCAAAGAA
rBai3-R	ACTGAGCATGTGCTCCACTG
rGAPDH-F	CTCATGACCACAGTCCATGC
rGAPDH-R	TTCAGCTCTGGGATGACCTT
rIL1β-F	CTGTGACTCGTGGGATGATG
rIL1β-R	GGGATTTTGTCGTTGCTTGT
rIL6-F	CCGGAGAGGAGACTTCACAG
rIL6-R	ACAGTGCATCATCGCTGTTC
rTNFα-F	AGATGTGGAACTGGCAGAGG
rTNFα-R	CCCATTTGGGAACTTCTCCT
riNOS-F	AGGGAGTGTTGTTCCAGGTG
riNOS-R	TCCTCAACCTGCTCCTCACT
rIL10-F	CCTGCTCTTACTGGCTGGAG
rIL10-R	TGTCCAGCTGGTCCTTCTTT
rArg1-F	TATCGGAGCGCCTTTCTCTA
rArg1-R	ACAGACCGTGGGTTCTTCAC
rMrc1-F	CAAGGAAGGTTGGCATTTGT
rMrc1-R	CAAAGGAACGTGTGCTCTGA

2.5 | Immunohistology staining

The WT and KO rats at 8 months of age (n = 5 per group) were killed, and the brain tissues were collected. The brain tissues were fixed in 4% paraformaldehyde for 24 h and immersed in 20% sucrose followed by 30% sucrose. The coronal frozen sections (25 μm thick) were prepared according to the methods previously reported.[23] The immunohistology staining of microglia was performed using the protocol provided by the anti-Iba1antibody manufacturer. Briefly, the sections were dewaxed and hydrated in phosphate-buffered saline, blocked with 10% normal goat serum, and then incubated overnight at 4°C with anti-Iba1 antibody (ab178847, 1:200, Abcam). The sections were then incubated for 20 min at 37°C with horseradish peroxidase (HRP)-conjugated goat antirabbit IgG (PV-9001, 1:200, ZSGB-Bio). The secondary antibody was visualized with the substrate of DAB (3,3'-diaminobenzidine) (ZLI-9018, 1:50, ZSGB-Bio). The sections were mounted in a mounting buffer with DAPI (4,6-Diamidino-2-phenylindole,dihydrochloride) (ZLI-9557, ZSGB-Bio). The images of the sections were scanned with a digital slide scanner (Pannoramic 250 FLASH, 3DHISTECH) and captured by case viewer software. The total number of ramified, hypertrophic, and amoeboid microglia were counted (40 fields from 3 rats), and the average cell body sizes were measured by image J (40 fields from 3 rats).

2.6 | Magnetic resonance imaging examination

A 7.0 T small animal magnetic resonance imaging (MRI) system (Varian, Palo Alto, CA, USA) was used for MRI examination of the WT (n = 5) and KO rats (n = 4) at 4 months of age. The rats were anesthetized with 2% isoflurane in medical oxygen (1 L/min). The coronal T2-weighted images were obtained with fast spin-echo sequences. The parameters were set as follows: field of view = 35 × 35 mm; no slice = 20; slice thickness = 1 mm; TR = 3000 ms; TE = 18.0 ms; image matrix = 256 × 256; and number of averages = 10. The HPC areas were drawn on the T2 images, and their volumes were estimated by the software of Vnmrj (Varian).

2.7 | Sholl analysis and dendritic spine counting of neuron

The fresh brain tissues were sampled from WT (n = 3) and KO (n = 3) rats at 8 months of age. The experiments were performed according to the protocol of the Golgi Stain Kit (PK401, FD Neurotechnologies). Briefly, the brain tissues were treated twice in a premixed solution of A and B, followed by solution C. The tissues were snap-frozen in isopentane at −80°C and then cut into 90-μm-thick sections using a cryostat microtome at −22°C (Leica, Wetzlar, Germany). The sections were sequentially treated with solutions of C, D, and E to finish the Golgi staining. The sections were then dehydrated, cleared, and mounted with gum as a standard pathological procedure. Sections were scanned, and Z-stacking images were obtained on a scanner (Pannoramic 250 FLASH, 3DHISTECH). At least 30 images per slice on a Z-stack mode were captured to establish three-dimensional (3D) images of dendrites. The 3D images of pyramidal neurons in the cortex (9 neurons per group) were used for Sholl analysis using Image J.[26,27] The number of intersections with the Sholl circles was counted, which represented the neural complexity. The dendritic segments 10 μm long from the tip of the basal dendrite were intercepted from 3D images of pyramidal neurons. At least 11 segments in each group were used to count the dendritic spines by Reconstruct 1.1.0.0. Software as previously reported.[28,29] The number of the spines represented the status of neuron and synapse integrity.

2.8 | Behavior analysis

The behavior of rats was determined at 8 months of age by open field test, Morris water maze (MWM) test, and Y maze test in a specific pathogen-free (SPF) facility at standard conditions.

For the open field test, the rats (WT, n = 30; KO, n = 15) were gently placed in the center zone of the open field box (80 × 80 × 35 cm) and were allowed to explore freely for 5 min in the box. The arena was divided into three areas including periphery (zone 1), transition (zone 2), and center (zone 3). The motion trail of each rat was recorded for 5 min using a camera. The moving distances, velocity, and frequencies in the three zones of the rats were, respectively, estimated with VisuTrack software (XinRuan, Shanghai, China).

The MWM test was modified from a protocol of our previous study.[30] A large round pool with a diameter of 150 cm and height of 60 cm was divided into four zones. A hidden platform in water was placed in the target zone of the pool. The rats (WT, $n=27$; KO $n=12$) were placed in the pool and allowed to swim for 60 s once, which was repeated twice a day. This operation lasted for 5 days, which would allow the rats to set up spatial memory about the coordinates of the target zoon and the hidden platform. The time to find the platform was recorded as latency, which represented the learning ability of the rats. On day 6, the hidden platform was removed. The rats were placed in contralateral zoon of the target zoon swim for 120 s. The platform crossing number and target zoon duration were recorded using a video tracking system to estimate the spatial memory of the rats.

The Y maze test was performed according to the methods of our previous study.[31] Briefly, the three arms of the maze apparatus (60 × 15 × 20 cm) were conveniently marked as A, B, and C. The rats (WT, $n=25$; KO, $n=16$) were released at the end of one arm and allowed to explore freely for 5 min among the three arms. The total moved distances, entry numbers, and sequences in different arms in 5 min were recorded by VisuTrack software. The correct spontaneous alternation between arms, such as A–B–C or B–C–A or C–A–B, were counted and calculated using the formula: the spontaneous alteration (%) = alternative number/(total entry number − 2) × 100%, which reflected the working memory. Between the two tests, the Y maze was cleaned with 75% ethanol.

2.9 | Statistical analysis

All of the data were expressed as mean ± SD, and an unpaired *t*-test was used for comparison between only two groups. The data of crossing in three zones of open filed box were analyzed using multiple *t*-tests. The 5-day escape latency data from MWM tests were analyzed using repeated measures of two-way analysis of variance (ANOVA), and the other data were analyzed by one-way ANOVA. The two-tailed *p* values less than 0.05 were considered statistically significant. Statistical analysis was performed using GraphPad Prism software (version 9).

3 | RESULTS

3.1 | Generation and identification of *C1ql3* KO rats

Before the generation of *C1ql3* KO rats, we detected the expression pattern of *C1ql3*, which might suggest some clues about its function. First, the expression data from Expression Atlas (https://asia.ensembl.org) showed that *C1ql3* expression was mainly confined to brain tissues of humans, F344 rats, and C57BL/6 mice (Figure 1A). The results of qRT-PCR showed that *C1ql3* was also mainly expressed in the brain tissues of Wister rats (Figure 1B). Second, in primary culture, both microglia and neurons expressed *C1ql3* and its receptor gene *Bai3* (Figure 1C,D). Third, we detected the *C1ql3* expression in a few brain samples from human Alzheimer's disease (AD), and the results showed that *C1ql3* mRNA levels were significantly decreased in AD brain samples compared with that of normal brain samples (Figure 1E; $n=8$, $p<0.01$). These results suggested that *C1ql3* mainly expressed in the brain was produced by both microglia and neurons and may be involved in AD.

The *C1ql3* KO Wistar rats were generated by the CRISPR/cas9 strategy, and seven heterozygous KO founders (3, 5, 7, 9, 10, 11, 13) were obtained from 14 litters (Figure 1F,G). The heterozygous founder rats 9 and 13 were selected for breeding, and founder rat 13 could be successfully passaged and generate homozygous KO rats, which had a deleted 631 bp fragment and an added stop codon at +61 bp of the open reading frame, which resulted in the loss of *C1ql3* protein in the brain tissues (Figure 1H). No obvious changes in feed, coat, and bodyweight (Figure 1I, $n=8$, not significant [ns]) were observed in KO rats compared with WT rats. The survival of *C1ql3* KO rats was monitored from birth to 12 months of age, and the results indicated that *C1ql3* KO did not affect the life span of rats. These results indicate that *C1ql3* KO rats were successfully generated, and *C1ql3* KO did not affect growth, development, and survival.

3.2 | *C1ql3* KO promotes the microglia activation

Microglia play significant noninnate immune roles and support the development, maintenance, homeostasis, and repair of the brain. The morphology of microglia may reflect its active status and is related to its function.[32] The ramified microglia have long thin branches and a small cell body, which secretes cytokines and chemically surveys the environment of the brain. The hypertrophic microglia are activated with short thick branches and an enlarged cell body, which are involved in phagocytosis, antigen presentation, and production of inflammatory factors. The amoeboid microglia have fewer or no branches and tend to phagocytose debris in the brain. Immunohistochemistry for IBA1 on brain sections was performed to investigate the effect of *C1ql3* KO on microglia. The results analysis of Iba1-positive microglia showed that the total number of microglia in KO brains did not differ from that of WT brains (Figure 2B; $n=30$, ns). However, the number of ramified microglia was significantly increased by 40% in the KO brain (Figure 2D; $n=30$, $p<0.01$), whereas the hypertrophic microglia were significantly decreased by 35% in the KO brain compared with the WT brain (Figure 2E; $n=30$, $p<0.01$). The average size of microglia in the KO brain also showed an increased tendency compared with that of the WT brain (Figure 2C; $n=40$, $p<0.05$). These results indicated that *C1ql3* loss affected microglia morphology, which may reflect the changes in microglia activation state induced

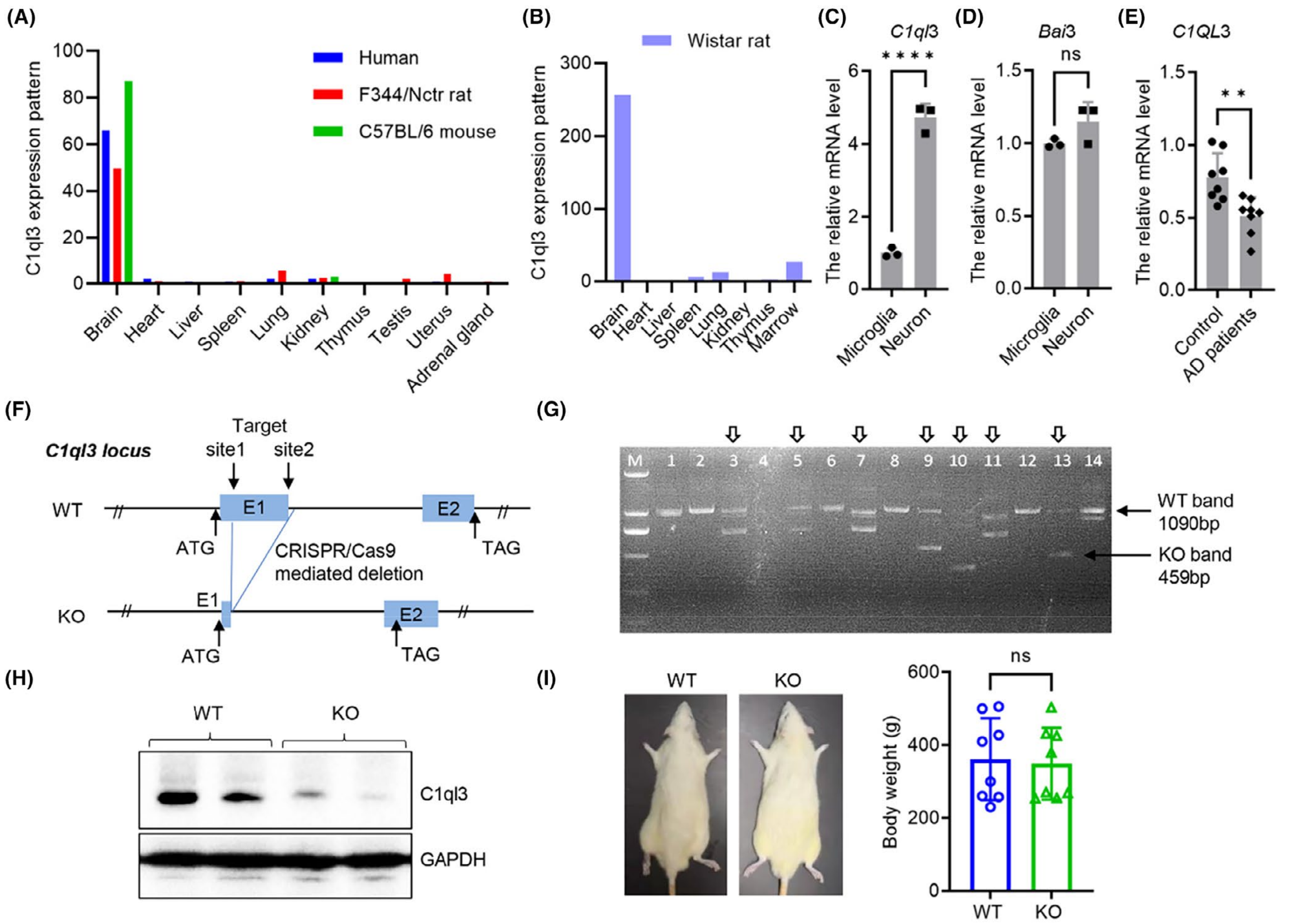

FIGURE 1 The expression of *C1ql3* in different tissues and the identification of knockout (KO) rats. (A) The *C1ql3* expression in different tissues from humans, rats, and mice was compared using the data obtained from Expression Atlas (https://asia.ensembl.org). (B) The tissue expression pattern of *C1ql3* mRNA in Wistar rats was confirmed with real-time polymerase chain reaction (RT-PCR) ($n = 3$). (C) The *C1ql3* mRNA levels in primary culture microglia and neurons were detected using RT-PCR ($n = 3$). (D) The *Bai3* mRNA levels in primary culture microglia and neurons were detected using RT-PCR ($n = 3$). (E) The *C1ql3* mRNA levels in control and Alzheimer's disease (AD) brain samples were compared using RT-PCR ($n = 8$). (F) The *C1ql3* were knocked out in Wistar rats by the CRISPR/cas9 strategy. (G) Fourteen litters were genotyped using PCR and confirmed by DNA sequencing. Among them, seven heterozygous KO rats (indicated by hollow arrow) were obtained, and the founder 13 could be passaged and the offspring were used for follow-up studies. (H) The expression of the *C1ql3* protein was detected in the homozygous *C1ql3* KO rats. (I) The growth status of KO rats was observed, including feed, coat, and bodyweight ($n = 8$). ns, not significant. **$p < 0.01$; ****$p < 0.0001$.

by *C1ql3* KO. However, although the microglia activation was affected by the deletion of *C1ql3*, the expression of TNF-α, iNOS, IL-1β, IL-6, Mrc1, and Arg1 did not change in KO brains compared with that of WT brains (Figure 3A–F; $n = 6$ or 8, ns). Only the levels of IL-10, an anti-inflammatory factor, were increased by 55% in the KO brain compared with that of the WT brain (Figure 3G; $n = 6$ or 8, $p < 0.05$). These results suggest that *C1ql3* KO might be positively associated with microglial M2 polarization, which was consistent with the results of one recent study.[33]

To further explore the effect of *C1ql3* KO on microglia under inflammatory conditions, LPS intraperitoneal injection was administered once, and the brains were extracted and sectioned into 25-μm coronal sections after 1 week. The results showed that, under LPS stimulus condition, the number of ramified microglia and hypertrophic microglia was significantly decreased by 74% and 68%, respectively, in the KO brain (Figure 2D,E; $n = 30$, $p < 0.001$; Table 2), whereas the amoeboid microglia in KO brain were significantly increased by 74% compared with the WT brain (Figure 2F; $n = 30$, $p < 0.001$; Table 2). The expression of TNF-α, iNOS, IL-1β, IL-6, Mrc1, and IL-10 in the KO brain with LPS stimulus did not differ from that of the WT brain with LPS stimulus (Figure 3A–E,G; $n = 6$ or 8, $p < 0.05$; Table 2), whereas the levels of Arg1, an anti-inflammatory factor, were significantly increased by 16% in the KO brain compared with that of the WT brain (Figure 3F; $n = 6$ or 8, $p < 0.05$; Table 2).

After the LPS stimulus, both WT and KO microglia were activated by LPS, indicated by increasing the amoeboid type and inflammatory factor expression such as IL-1β (Figure 3; Table 2). Of note, the activation of KO microglia induced by LPS appeared to be stronger than WT microglia, indicated by increasing the amoeboid type

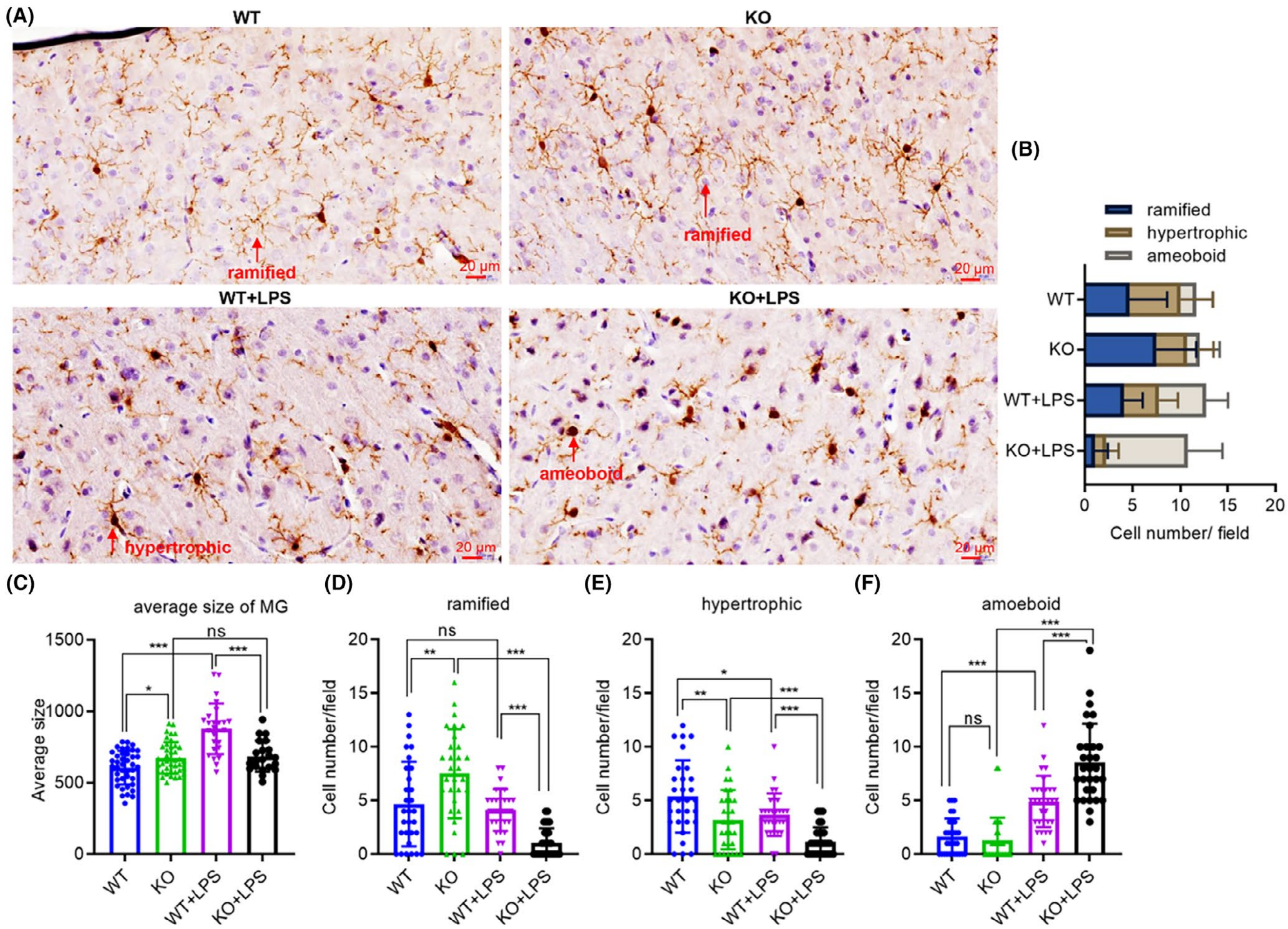

FIGURE 2 The morphological observation of the microglia of wild-type (WT) and knockout (KO) rats. (A) The brain samples were collected from WT and KO rats at 8 months of age. The brain sections were prepared and stained with Iba1 antibody to mark the microglia cells. The presentative images of microglia in the brain cortex from WT and KO rats with or without lipopolysaccharide (LPS) stimulus were shown (scale = 20 μm). Red arrows marked different microglial types, including ramified, hypertrophic, and amoeboid microglia. (B) The total number of microglia was counted and compared between WT and KO brains with or without LPS stimulus ($n = 30$ per group). (C) The average sizes of the cell body of microglia were measured by Image J (WT, $n = 40$; KO, $n = 40$; WT + LPS, $n = 25$; KO + LPS, $n = 21$). (D–F) The number of ramified, hypertrophic, and amoeboid microglia was compared between WT and KO brains with or without LPS stimulus ($n = 30$ per group). ns, not significant. *$p < 0.05$, **$p < 0.01$, ***$p < 0.001$.

and anti-inflammatory factor Arg-1 expression in KO + LPS microglia compared with WT + LPS microglia (Figure 3; Table 2).

Taken together, these results suggest that *C1ql3* KO increases microglial anti-inflammatory activity without pathologic stimulus indicated by higher IL-10 level, whereas *C1ql3* KO promotes both microglial amoeboid-like polarization and anti-inflammatory activity under LPS stimulation conditions.

3.3 | *C1ql3* KO damages neuronal integrity

The WT and KO rats were first applied to MRI examination to estimate the volumes of HPC of the rats. The rats were then killed, and the whole brains were stripped and weighed. The results showed that both HPC volumes and brain weight of KO rats did not differ from that of WT rats (Figure 4A–C; WT, $n = 5$; KO, $n = 4$; ns). To analyze the neuronal integrity, the neuronal complexity and spines in the cortex were detected by performing Golgi staining. The Sholl analysis of Golgi-stained neurons showed that the intersection number of KO neurons was significantly reduced compared with WT neurons (Figure 5A,C; $n = 9$ per group, $p < 0.01$). This result indicated that neuronal complexity was damaged by the *C1ql3* KO. The dendritic segments 10 μm long from the tip of the basal dendrite were amplified, and the spines with different morphology as filo, long thin, thin, stub, mush, and branch were observed and counted. The result showed that the total number of spine protrusions (Prots) of KO neurons was significantly reduced (Figure 5B,D; $n = 11$ per group, $p < 0.001$), especially the mush and branch spines on KO neurons was significantly reduced compared with that of WT neurons (Figure 5B,D; $n = 11$ per group, $p < 0.05$). The alteration in dendritic arborization and the decrease in spine density in KO brains suggest that the *C1ql3* KO interrupted neuronal integrity.

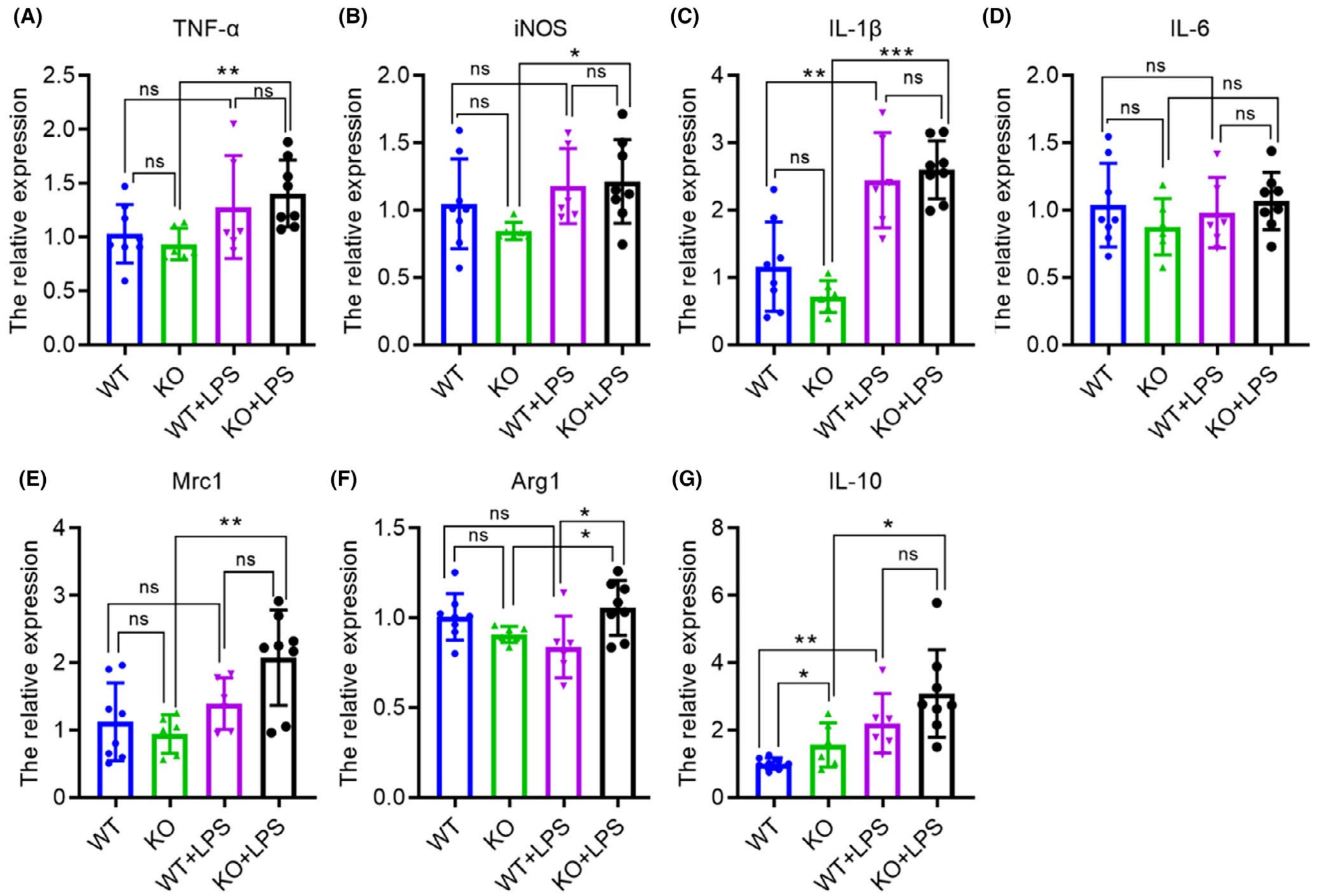

FIGURE 3 The cytokine expression of the brain tissues of wild-type (WT) and knockout (KO) rats. (A–D) The total RNA of the cortex and hippocampus tissues was isolated from WT and KO rats at 8 months of age. The pro-inflammatory factor levels of TNF-α, iNOS, IL-1β, and IL-6 in WT, KO, WT + lipopolysaccharide (LPS), and KO + LPS brain samples were detected using real-time polymerase chain reaction (RT-PCR) (WT, $n = 8$; KO, $n = 6$; WT + LPS, $n = 6$; KO + LPS, $n = 8$). (E–G) The anti-inflammatory factor levels of Mrc1, Arg1, and IL-10 in WT, KO, WT + LPS, and KO + LPS brain samples were detected using RT-PCR (WT, $n = 8$; KO, $n = 6$; WT + LPS, $n = 6$; KO + LPS, $n = 8$). ns, not significant. *$p < 0.05$, **$p < 0.01$, ***$p < 0.001$.

TABLE 2 The changes in microglial morphology and inflammatory factors in WT and KO rat brain with or without LPS stimulus.

Group comparison	KO versus WT	KO + LPS versus WT + LPS	WT + LPS versus WT	KO + LPS versus KO
Resting	Ramified ↑**	Ramified ↓***	Ramified ↓ns	Ramified ↓***
Activated	Hypertrophic ↓** Amoeboid ↓ns	Hypertrophic ↓*** Amoeboid ↑***	Hypertrophic ↓* Amoeboid ↑***	Hypertrophic ↓*** Amoeboid ↑***
Pro-inflammatory	TNF-α↓ns iNOS↓ns IL-1β↓ns IL-6↓ns	TNF-α↑ns iNOS↑ns IL-1β↑ns IL-6↑ns	TNF-α↑ns iNOS↑ns IL-1β↑** IL-6↑ns	TNF-α↑** iNOS↑* IL-1β↑*** IL-6↑ns
Anti-inflammatory	Mrc1↓ns IL-10↑* Arg1↓ns	Mrc1↑ns IL-10↑ns Arg1↑*	Mrc1↓ns IL-10↑** Arg1↓ns	Mrc1↑** IL-10↑* Arg1↑*

Abbreviations: ↓, downregulated; KO, knockout; LPS, lipopolysaccharide; ns, not significant; ↑, upregulated; WT, wild type.
*$p < 0.05$; **$p < 0.01$; ***$p < 0.001$.

3.4 | *C1ql3* KO causes abnormal behaviors in rats

To investigate the behaviors of KO rats, WT and KO rats were comparatively applied to the open field test, MWM test, and Y maze test. The open field test showed that the KO rats were hyperactive, had a longer path length, displayed higher moving speed, and increased frequencies crossing the zones (Figure 6A–D; WT, $n = 30$; KO, $n = 15$; $p < 0.05$). No significant cognitive defect

FIGURE 4 The magnetic resonance imaging (MRI) examination of the hippocampus (HPC) volumes of wild-type (WT) and knockout (KO) rats. (A) WT and KO rats at 4 months of age were anesthetized with 2% isoflurane, and the serial coronal T2 images were obtained from MRI. The representative images of WT and KO brains (WT, $n=4$; KO, $n=4$) are shown, and blue-circled regions are HPC area (scale = 5 mm). (B) HPC volumes of WT and KO brains were calculated and compared (WT, $n=5$; KO, $n=4$). (C) After the MRI examination, the whole brains were stripped and weighed (WT, $n=5$; KO, $n=4$). ns, not significant.

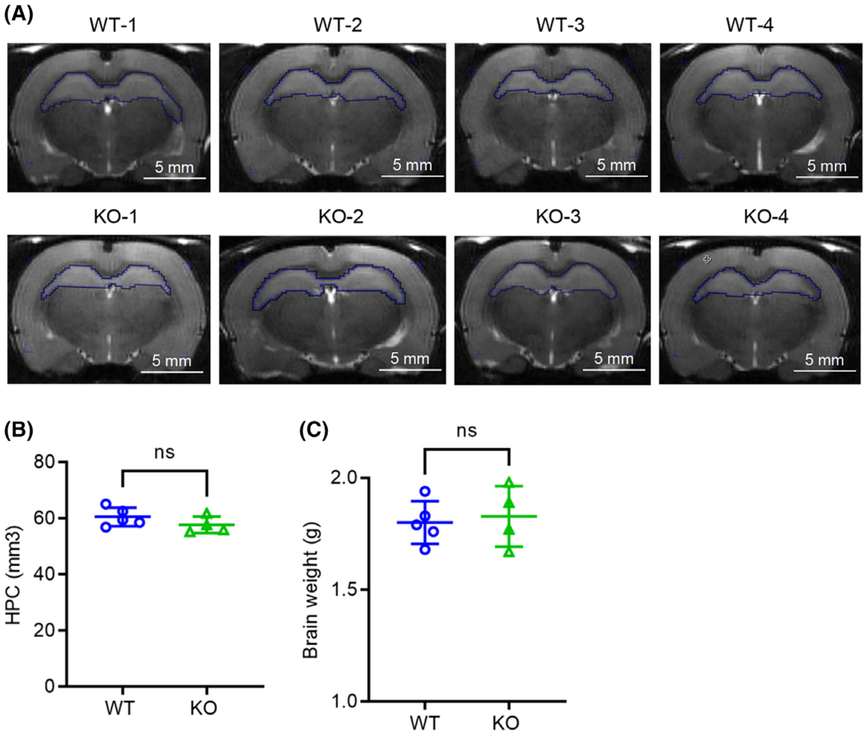

was noticed in KO rats compared with WT rats in the MWM test (Figure 6E–H; WT, $n=30$; KO, $n=15$; ns). However, the impairment in the short working memory of KO rats was observed, indicating significantly reduced spontaneous alteration compared with WT rats in the Y maze test (Figure 6I–K; WT, $n=30$; KO, $n=15$; $p<0.01$). The results suggested that *C1ql3* KO altered natural behavior and interrupted short working memory.

4 | DISCUSSION

Although C1QL3 is a brain-specific expression protein in humans and rodents,[1,2] the reports about its function are still limited. The role of *C1ql3* KO in regulating synapse density has been demonstrated in mice.[1,8] Similarly, we observed that mush and branch spines were significantly reduced in KO rat neurons compared with WT rat neurons (Figure 5B,D; $n=11$ per group, $p<0.05$), which resulted in the fact that the total number of spines was significantly reduced in KO rat neurons relative to WT rats (Figure 5B,D; $n=11$ per group, $p<0.001$). It was reported that the BAI3 protein, the receptor of C1QL3, regulated synaptogenesis required for normal brain function.[34] Therefore, it was a possible mechanism that the impairment of the *C1ql3*/*Bai3* signal pathway was involved in the regulation of synapse damage in *C1ql3* KO rats. Importantly, we also observed that neuronal complexity was interrupted by the *C1ql3* KO, indicated by the results of the Sholl analysis (Figure 5A,C; $n=9$ per group, $p<0.01$). Neuronal functions are closely dependent on neuronal integrity, including dendritic architecture, synaptic structure, and plasticity.[35–37] These results highlight the important role of C1QL3 in maintaining neuronal architecture and brain function.

In physiological conditions, microglia are critical for proper neuronal function in the brain, including the regulation of programmed cell death, neurite formation, synaptic homeostasis, and synaptogenesis.[38] In pathological conditions, microglial activation is closely correlated with many pathological changes and influences disease progression by its anti-inflammatory or pro-inflammatory responses in brain diseases, such as AD, motor neuron disease, and Parkinson's disease.[39,40] The morphology of microglia corresponds to its active status and is related to its function.[32,41] To date, only one previous study of traumatic brain injury in mice demonstrates the indirect association of downregulating *C1ql3* expression with microglial polarization after curcumin treatment.[33] Here, we showed the direct effect of *C1ql3* KO on microglia morphology and activation under both physiological and pathological conditions. Our results showed that *C1ql3* was not only expressed in neurons but also expressed in microglia (Figure 1C). Importantly, *Bai3*, which had been validated as a high-affinity receptor of *C1ql3*,[11,12] was also expressed in microglia (Figure 1D). Therefore, we first analyzed the microglial morphology and activation status of KO brains and found that the deletion of *C1ql3* significantly increased the number of ramified microglia (Figure 2D; $n=30$, $p<0.01$) and decreased the number of hypertrophic microglia (Figure 2E; $n=30$, $p<0.01$), suggesting the possible role of *C1ql3* in controlling the physiological status of brain microglia. Furthermore, we evaluated the effects of *C1ql3* KO on microglia under LPS inflammatory stimulus. The results indicate that *C1ql3* KO rats had more amoeboid microglia types and higher anti-inflammatory factor Arg-1 expression after LPS stimulation compared with the WT

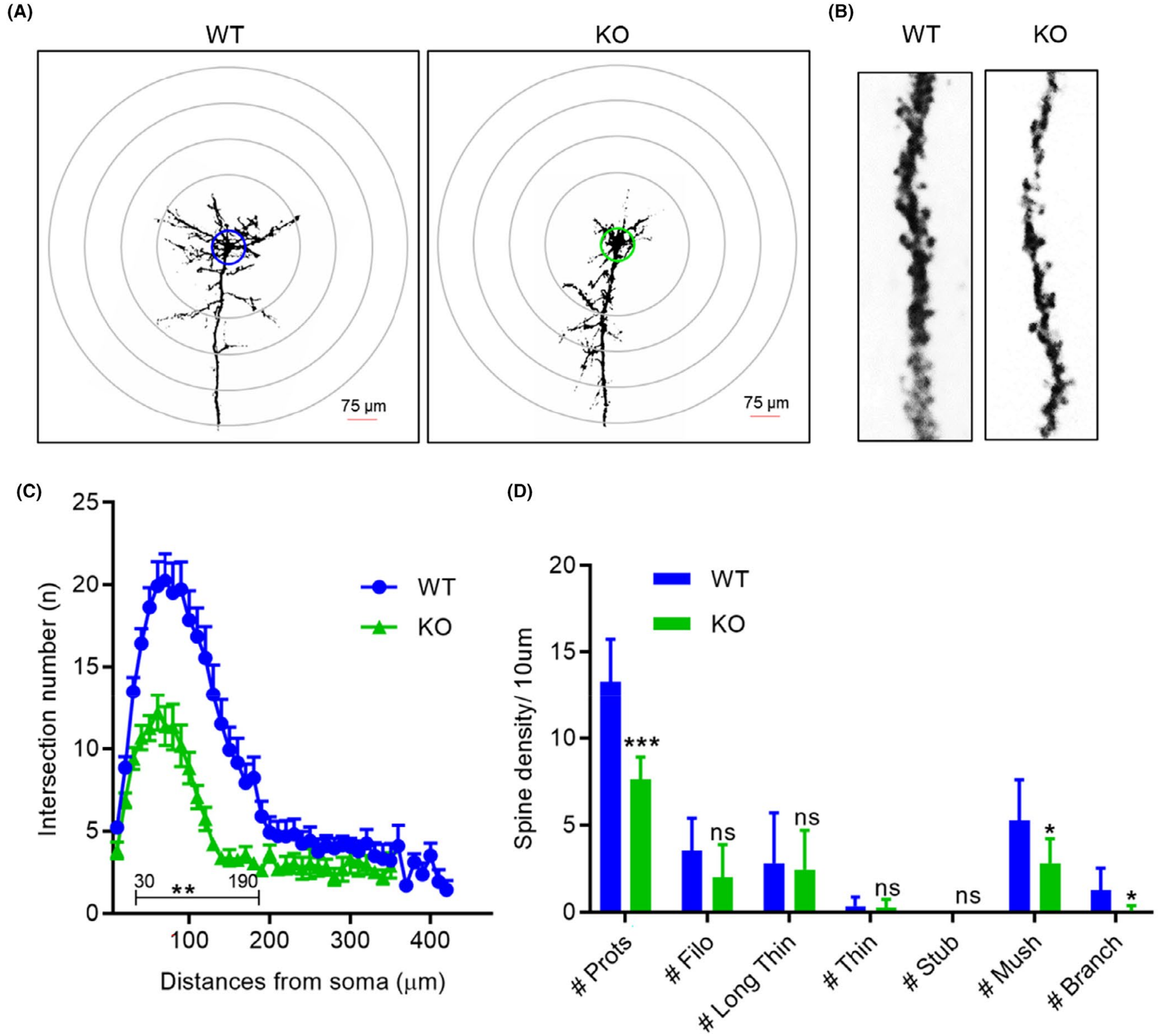

FIGURE 5 The detection of the neuronal integrity of wild-type (WT) and knockout (KO) rats. (A), (C) The thick brain sections from WT and KO rats at 8 months of age were stained with a Golgi staining kit. The binary images of neurons in the WT and KO cortex were randomly acquired, and the intersection number of neurons was determined by Sholl analysis, which indicated the neuronal complexity ($n = 9$ per group). Scale bar = 75 μm. (B), (D) The Z-stack images of basal dendrites on the neurons from WT and KO cortices were acquired by a digital slide scanner, and the total number of dendritic spines on 10-μm basal dendrites was counted using RECONSTRUCT software ($n = 11$ per group). *$p < 0.05$, **$p < 0.01$, ***$p < 0.001$; ns, not significant.

rats with the LPS stimulus (Figures 2 and 3; Table 2), suggesting the effects of *C1ql3* KO on the microglial polarization under pathological conditions. Taken together, the process of microglia activation was affected by *C1ql3* KO, suggesting that the regulation of microglia was a possible mechanism for *C1ql3* involved in neural activity.

C1ql3 KO rats displayed hyperactivity including a longer path length, higher moving speed, and increased frequencies crossing the zones in the open field test (Figure 6A–D; WT, $n = 30$; KO, $n = 15$; $p < 0.05$), which was an attention-deficit hyperactivity disorder (ADHD)-like phenotypes.[42] The circadian rhythm abnormality is a clinical feature of ADHD,[43] and the *C1ql3* plays a role in circadian behaviors.[8,9,17] We speculate that hyperactivity induced by *C1ql3* KO might be due to the interruption of circadian rhythm in rats.

The Y maze can be used to assess short-term working memory in rodents, and the spontaneous alternation between the arms reflects the status of working memory and prefrontal cortical functions.[44] The *C1ql3* KO rats showed a significant decrease in spontaneous alternation in the Y maze test relative to WT rats (Figure 6K; WT, $n = 25$; KO, $n = 16$; $p < 0.01$). The results suggest that abnormality of short-term working memory and prefrontal cortical function may

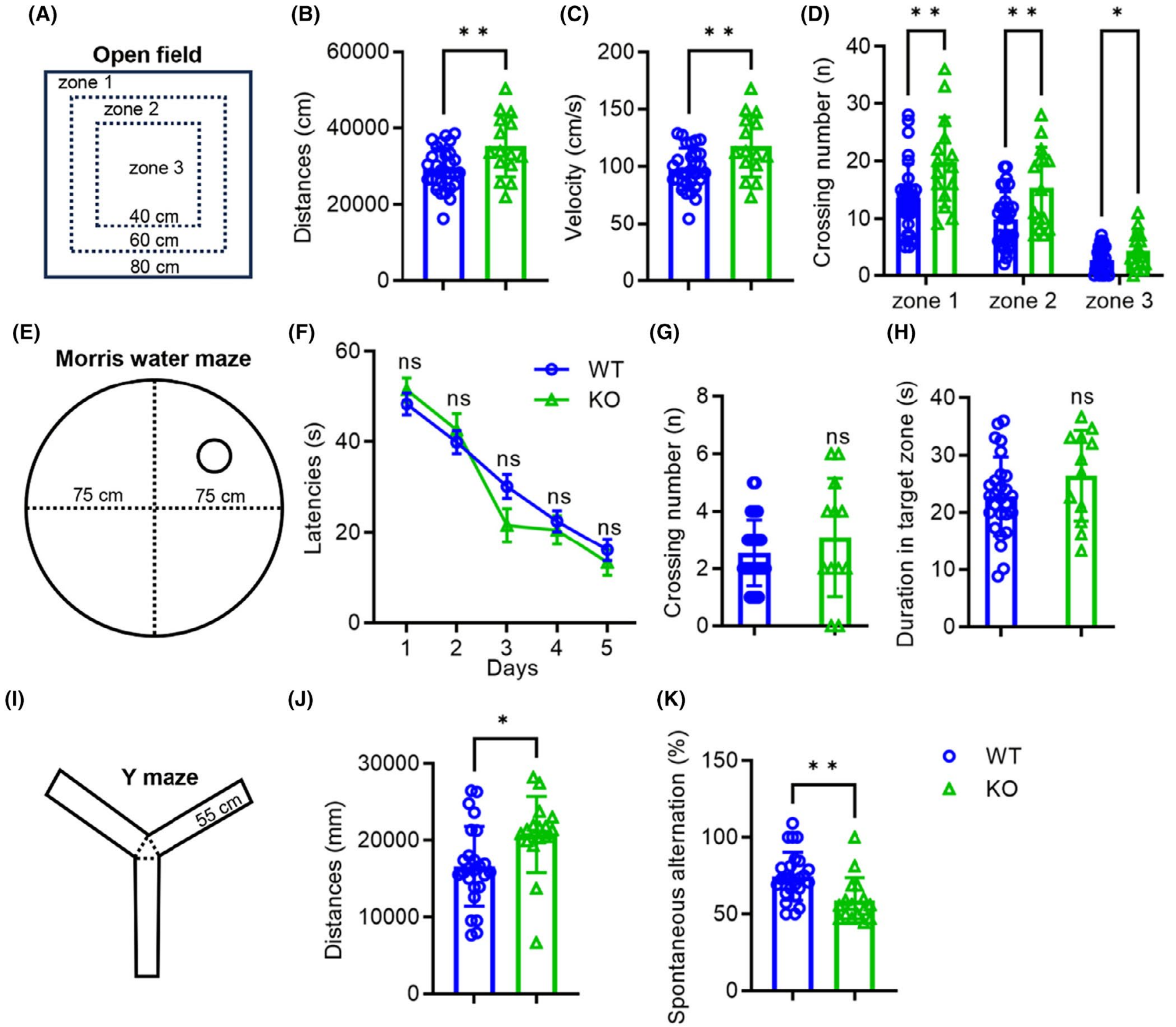

FIGURE 6 The behavior analysis of wild-type (WT) and knockout (KO) rats. The WT and KO rats were applied to three different behavior tests to estimate their cognitive ability. (A–D) In the open field test, the total distances moved, velocity, and frequency in zone 1, zone 2, and zone 3 were used to evaluate the hyperactive behavior (WT, $n=30$; KO, $n=15$). (E–H) In the Morris water maze test, the escape latencies to find the platform during the training phase, the crossing number over the platform area, and the duration in the target zone during the examination phase were used to evaluate the spatial learning and memory (WT, $n=27$; KO, $n=12$). ns, not significant. (I–K) The short working memory of rats (WT, $n=25$; KO, $n=16$) was evaluated using spontaneous alteration (%) in the Y maze, and the total distances moved in the maze were also shown here. $^*p<0.05$, $^{**}p<0.01$; ns, not significant.

exist in *C1ql3* KO rats, which may be caused by the neuronal and synaptic damage observed in KO rats.

There have been several studies based on *C1ql3* KO mice,[7–10,45] whereas we generated *C1ql3* KO rats for the first time in the present study. We have summarized and compared the phenotype difference between *C1ql3* KO rats and *C1ql3* KO mice in Table 3. In brief, they both have increased activities and decreased synapse densities. Working memory impairment was observed in *C1ql3* KO rats, whereas fear memory impairment was observed in *C1ql3* KO mice. However, the effect of *C1ql3* KO on glucose and lipid metabolism in rats should be investigated in the future studies.

There are three limitations of this study that should be noted. First, single-cell sequencing should be applied to explore microglia diversity to determine the precise effect of *C1ql3* KO on the microglia. Second, neuron-specific KO or glial-specific KO animal model should be used for studying the effect of *C1ql3* on neurons or microglia. Third, primary neuron or microglia cells should be isolated from KO rats to study the effect of *C1ql3* KO in vitro. In our future work, we intend to investigate the effect of *C1ql3* on neuronal or glial cells using selective KO animal models and primary culture in combination with single-cell sequencing.

TABLE 3 The comparison of phenotype features between *C1ql3* KO rats and *C1ql3* KO mice.

Phenotype	*C1ql3* KO rats	*C1ql3* KO mice
Activity	Increased	Increased
Body weight	Not changed	Decreased
Glucose and lipid metabolism	Not detected	Improved
Synapse	Decreased	Decreased
Microglia activation	Affected	Not detected
Fear memory	Not detected	Impaired
Working memory	Impaired	Not detected
Spatial memory	Not changed	Not detected

Abbreviations: KO, knockout; ns, not significant; WT, wild type.

5 | CONCLUSION

In conclusion, *C1ql3* KO interrupts the neuronal integrity, affects the microglial morphology and polarization, and causes hyperactive behavior and impaired working memory in rats, highlighting the role of C1ql3 protein in regulating the structure and function of neurons and microglia.

AUTHOR CONTRIBUTIONS

LFZ and FFG designed the study and wrote the paper. WD designed gRNA targeting to *C1ql*3 gene. LZ, WD and HXS performed the experiments. SG and JWL performed the genotyping and management of the knockout rats. QK did the bioinformatical analysis. LZ analyzed the data and revised the paper. All authors have approved the final manuscript.

ACKNOWLEDGEMENTS

The authors thank Kai Gao and Xudong Shi for assistance with MRI scan. This research was support by the National Natural Science Foundation (31970508) and The National Key Research and Development Program of China (2022YFF0710702).

FUNDING INFORMATION

The present work was supported by the National Natural Science Foundation (31970508) and the National Key Research and Development Program of China (2022YFF0710702).

CONFLICT OF INTEREST STATEMENT

None.

ETHICS STATEMENT

All rats used in this study were bred in an SPF facility, and the rats-related experiments were approved by the Animal Care and Use Committees of the Institute of Laboratory Animal Science of Peking Union Medical College (approval no. MYW20012).

ORCID

Li Zhang https://orcid.org/0000-0002-3919-3247
Hanxuan Sheng https://orcid.org/0000-0003-2593-4697
Lianfeng Zhang https://orcid.org/0000-0002-5774-2924

REFERENCES

1. Iijima T, Miura E, Watanabe M, Yuzaki M. Distinct expression of C1q-like family mRNAs in mouse brain and biochemical characterization of their encoded proteins. *Eur J Neurosci*. 2010;31(9):1606-1615.
2. Yuzaki M. The C1q complement family of synaptic organizers: not just complementary. *Curr Opin Neurobiol*. 2017;45:9-15.
3. Wei Z, Peterson JM, Wong GW. Metabolic regulation by C1q/TNF-related protein-13 (CTRP13): activation OF AMP-activated protein kinase and suppression of fatty acid-induced JNK signaling. *J Biol Chem*. 2011;286(18):15652-15665.
4. Wang C, Chao Y, Xu W, et al. CTRP13 preserves endothelial function by targeting GTP cyclohydrolase 1 in diabetes. *Diabetes*. 2020;69(1):99-111.
5. Erbas IM, Paketçi A, Turan S, et al. Low complement C1q/TNF-related protein-13 levels are associated with childhood obesity but not binge eating disorder. *J Clin Res Pediatr Endocrinol*. 2022;14(2):179-187.
6. Ramanadham S, Turk J, Bhatnagar S. Noncanonical regulation of cAMP-dependent insulin secretion and its implications in type 2 diabetes. *Compr Physiol*. 2023;13(3):5023-5049.
7. Matsuda K, Budisantoso T, Mitakidis N, et al. Transsynaptic modulation of kainate receptor functions by C1q-like proteins. *Neuron*. 2016;90(4):752-767.
8. Martinelli DC, Chew KS, Rohlmann A, et al. Expression of C1ql3 in discrete neuronal populations controls efferent synapse numbers and diverse behaviors. *Neuron*. 2016;91(5):1034-1051.
9. Chew KS, Fernandez DC, Hattar S, Südhof TC, Martinelli DC. Anatomical and behavioral investigation of C1ql3 in the mouse suprachiasmatic nucleus. *J Biol Rhythms*. 2017;32(3):222-236.
10. Wang CY, Liu Z, Ng YH, Südhof TC. A synaptic circuit required for acquisition but not recall of social transmission of food preference. *Neuron*. 2020;107(1):144-157.e4.
11. Bolliger MF, Martinelli DC, Sudhof TC. The cell-adhesion G protein-coupled receptor BAI3 is a high-affinity receptor for C1q-like proteins. *Proc Natl Acad Sci U S A*. 2011;108(6):2534-2539.
12. Hamann J, Aust G, Araç D, et al. International union of basic and clinical pharmacology. XCIV. Adhesion G protein-coupled receptors. *Pharmacol Rev*. 2015;67(2):338-367.
13. Bhangoo SK, Swanson GT. Kainate receptor signaling in pain pathways. *Mol Pharmacol*. 2013;83(2):307-315.
14. Haitina T, Olsson F, Stephansson O, et al. Expression profile of the entire family of adhesion G protein-coupled receptors in mouse and rat. *BMC Neurosci*. 2008;9:43.
15. Kee HJ, Ahn KY, Choi KC, et al. Expression of brain-specific angiogenesis inhibitor 3 (BAI3) in normal brain and implications for BAI3 in ischemia-induced brain angiogenesis and malignant glioma. *FEBS Lett*. 2004;569(1–3):307-316.
16. Thomas M, Snead D, Mitchell D. An investigation into the potential role of brain angiogenesis inhibitor protein 3 (BAI3) in the tumorigenesis of small-cell carcinoma: a review of the surrounding literature. *J Recept Signal Transduct Res*. 2017;37(4):325-334.
17. Sticco MJ, Peña Palomino PA, Lukacsovich D, et al. C1QL3 promotes cell-cell adhesion by mediating complex formation between ADGRB3/BAI3 and neuronal pentraxins. *FASEB J*. 2021;35(1):e21194.
18. Galloway DA, Phillips AEM, Owen DRJ, Moore CS. Phagocytosis in the brain: homeostasis and disease. *Front Immunol*. 2019;10:790.
19. Brown GC, Neher JJ. Microglial phagocytosis of live neurons. *Nat Rev Neurosci*. 2014;15(4):209-216.
20. Fu R, Shen Q, Xu P, Luo JJ, Tang Y. Phagocytosis of microglia in the central nervous system diseases. *Mol Neurobiol*. 2014;49(3):1422-1434.

21. Vilalta A, Brown GC. Neurophagy, the phagocytosis of live neurons and synapses by glia, contributes to brain development and disease. *FEBS J*. 2018;285(19):3566-3575.
22. Ma Y, Chen W, Zhang X, et al. Increasing the efficiency of CRISPR/Cas9-mediated precise genome editing in rats by inhibiting NHEJ and using Cas9 protein. *RNA Biol*. 2016;13(7):605-612.
23. Zhang L, Sun C, Jin Y, et al. Dickkopf 3 (Dkk3) improves amyloid-beta pathology, cognitive dysfunction, and cerebral glucose metabolism in a transgenic mouse model of Alzheimer's disease. *J Alzheimers Dis*. 2017;60(2):733-746.
24. Zhang L, Dong W, Ma Y, et al. Pon1 deficiency promotes Trem2 pathway-mediated microglial phagocytosis and inhibits pro-inflammatory cytokines release in vitro and in vivo. *Mol Neurobiol*. 2022;59(7):4612-4629.
25. Goshi N, Morgan RK, Lein PJ, Seker E. A primary neural cell culture model to study neuron, astrocyte, and microglia interactions in neuroinflammation. *J Neuroinflammation*. 2020;17(1):155.
26. Binley KE, Ng WS, Tribble JR, Song B, Morgan JE. Sholl analysis: a quantitative comparison of semi-automated methods. *J Neurosci Methods*. 2014;225:65-70.
27. Sholl DA. Dendritic organization in the neurons of the visual and motor cortices of the cat. *J Anat*. 1953;87(4):387-406.
28. Shibata M, Pattabiraman K, Muchnik SK, et al. Hominini-specific regulation of CBLN2 increases prefrontal spinogenesis. *Nature*. 2021;598(7881):489-494.
29. Risher WC, Ustunkaya T, Singh Alvarado J, Eroglu C. Rapid Golgi analysis method for efficient and unbiased classification of dendritic spines. *PLoS ONE*. 2014;9(9):e107591.
30. Pang S, Sun C, Gao S, Yang Y, Pan X, Zhang L. Evodiamine derivatives improve cognitive abilities in APP(swe)/PS1(ΔE9) transgenic mouse models of Alzheimer's disease. *Animal Model Exp Med*. 2020;3(2):193-199.
31. Sheng H, Lu D, Qi X, et al. A neuron-specific Isca1 knockout rat developments multiple mitochondrial dysfunction syndromes. *Animal Model Exp Med*. 2023;6(2):155-167.
32. Cho K, Choi GE. Microglia: physiological functions revealed through morphological profiles. *Folia Biol (Praha)*. 2017;63(3):85-90.
33. Zhang M, Hao Z, Wu J, Teng Z, Qiu W, Cheng J. Curcumin ameliorates traumatic brain injury via C1ql3-mediated microglia M2 polarization. *Tissue Cell*. 2023;84:102164.
34. Sigoillot SM, Iyer K, Binda F, et al. The secreted protein C1QL1 and its receptor BAI3 control the synaptic connectivity of excitatory inputs converging on cerebellar Purkinje cells. *Cell Rep*. 2015;10(5):820-832.
35. Seong E, Yuan L, Arikkath J. Cadherins and catenins in dendrite and synapse morphogenesis. *Cell Adh Migr*. 2015;9(3):202-213.
36. Lemus HN, Warrington AE, Rodriguez M. Multiple sclerosis: mechanisms of disease and strategies for myelin and axonal repair. *Neurol Clin*. 2018;36(1):1-11.
37. Tavosanis G. Dendrite enlightenment. *Curr Opin Neurobiol*. 2021;69:222-230.
38. Wright-Jin EC, Gutmann DH. Microglia as dynamic cellular mediators of brain function. *Trends Mol Med*. 2019;25(11):967-979.
39. Ashford BA, Boche D, Cooper-Knock J, Heath PR, Simpson JE, Highley JR. Review: microglia in motor neuron disease. *Neuropathol Appl Neurobiol*. 2021;47(2):179-197.
40. Colonna M, Butovsky O. Microglia function in the central nervous system during health and neurodegeneration. *Annu Rev Immunol*. 2017;35:441-468.
41. Boche D, Perry VH, Nicoll JA. Review: activation patterns of microglia and their identification in the human brain. *Neuropathol Appl Neurobiol*. 2013;39(1):3-18.
42. Halperin D, Stavsky A, Kadir R, et al. CDH2 mutation affecting N-cadherin function causes attention-deficit hyperactivity disorder in humans and mice. *Nat Commun*. 2021;12(1):6187.
43. Becker SP. ADHD and sleep: recent advances and future directions. *Curr Opin Psychol*. 2020;34:50-56.
44. Kraeuter AK, Guest PC, Sarnyai Z. The Y-maze for assessment of spatial working and reference memory in mice. *Methods Mol Biol*. 2019;1916:105-111.
45. Chen F, Sarver DC, Saqib M, et al. CTRP13 ablation improves systemic glucose and lipid metabolism. *Mol Metab*. 2023;78:101824.

How to cite this article: Zhang L, Dong W, Li J, et al. *C1ql3* knockout affects microglia activation, neuronal integrity, and spontaneous behavior in Wistar rats. *Anim Models Exp Med*. 2025;8:332-343. doi:10.1002/ame2.12383